

Cavitation Erosion Properties of Microscale Texture Surfaces Induced by Laser Processing Technique

Enlan Zhao¹, Haifeng Yang^{2,3}, Bo Sun², Haoxue Chen²

¹*School of Mechanical & Electrical Engineering, Xuzhou University of Technology, XuZhou, 221111, China*

E-mail: yhf002@163.com

²*School of Mechatronic Engineering, China University of Mining & Technology, XuZhou, 221116, China*

³*Jiangsu Key Laboratory of Mine Mechanical and Electrical Equipment, China University of Mining & Technology, XuZhou, 221116, China*

Reasonable design and fabrication of surface topography can alleviate the cavitation erosion of material surface. The paper investigated the cavitation erosion behavior of plane and both laser induced microscale textures surface using ultrasonic vibratory apparatus and FLUENT software. Firstly, the pressure, velocity and vapor volume fraction distributions on plane were numerical simulated and cavitation erosion experiments of rectangular texture surface were carried out during the cavitation stabilization phase. Then, the influence of microscale texture periods on performance of cavitation erosion assistance was investigated. Lastly, effects of microscale texture types on cavitation erosion were conducted using three kinds of surfaces, plane, triangle texture surface and rectangular texture surface. We found that serious cavitation erosion occurred because of stronger water jet and shock wave impaction when larger bubbles collapse near the annular region, and dense cavitation pits formed in the circular region. For the performance of cavitation erosion assistance of different surfaces, there was an optimal period for both triangle (75 μm) and rectangular (400 μm) texture surfaces. Rectangular texture surface had better performance of cavitation erosion resistance compared to the other two surfaces.

DOI: 10.2961/jlmn.2018.03.0016

Keywords: cavitation erosion, laser processing, rectangular texture, triangle texture, numerical simulation

1. Introduction

Microscale texture surface has good properties such as friction reduction, super wettability, drag reduction, etc. [1-3]. Various methods, such as ion-beam texturing [4], mechanical processing [5], template printing [6], have been used to fabricate microscale and nanoscale structures. Compared with above discussed methods, laser processing technique has many advantages, such as adaptability for extensive materials, operability for many kinds of microstructures, high efficiency and low cost [7-9]. However, in technical literature there is very little information regarding the cavitation erosion behavior of laser induced microstructures on material surface.

Cavitation erosion is a process of the formation and rapid collapse of bubbles where there is a considerable local reduction in the pressure. When the collapse occurs near or close to a technical surface, this phenomenon can lead to significant material losses and even to the replacement of parts and components. Cavitation erosion was known as an important surface damage for equipment operating in hydraulic systems. A wide range of studies have been made all aiming toward reducing cavitation erosion, such as laser processing [10], coating technique [11], expensive materials [12] and ion implantation [13]. L.

Zhang proved the effects of laser shock processing on electrochemical corrosion resistance of weldments [10]. Alicja K. Krella presented the results of cavitation erosion of the Ti/TiN multilayer coatings deposited on the X6CrNiTi18-10 steel surface by means of cathodic arc evaporation PVD method [11]. Jinjun Lu has investigated the cavitation erosion resistance of one Yb- α -Sialon ceramic and two Dy- α -Sialon ceramics in deionized water [12]. Haibin Li showed the cavitation erosion behavior of CP-Ti sample after gas nitriding process as a result of compound layer with a hard, dense and free-defects microstructure formed on the surface [13].

Surface topography is a very important factor affecting surface cavitation, which has been investigated preliminary around the world. Y.J. Li showed that surface topography manufactured by formed cutter had remarkable influences on the incubation of cavitation erosion [14]. The results showed that reasonable design of surface topography can alleviate the formation, transportation, growth and collapse of the cavities, and finally reduce surface cavitation erosion. Therefore, the paper investigated the cavitation erosion behavior of plane and both laser induced texture surfaces using experimental and numerical simulation methods.

2. Methods

In the experimental process adopting ultrasonic vibratory cavitation erosion apparatus, a large number of bubbles with uneven spatial distribution were formed between the horn and specimen. Meanwhile, the time for the forming and breaking of bubble is in the level of sub-microsecond. It is very difficult to real-time observe its generation, breaking and distribution adopting the experimental method. FLUENT is a popular commercial CFD package internationally. Because of adopting multiple solutions and grid convergence techniques, FLUENT can achieve the best speed of convergence and the precision of solution. FLUENT software contains rich and advanced turbulence models, enabling ours to accurately simulate non-viscous, laminar and turbulent flows. Therefore, the flow fields on the specimen surface during ultrasonic cavitation were simulated by FLUENT software, where standard wall function was adopted for near wall, unsteady calculation was used and the acceleration was set to 9.81 m/s^2 . There were three kinds of $k-\varepsilon$ turbulence models in FLUENT software, such as standard $k-\varepsilon$, RNG $k-\varepsilon$ model and realizable $k-\varepsilon$ model. The advantage of the realizable $k-\varepsilon$ model was a more accurate prediction of the divergence ratio of the flat and cylindrical jets. And it has good performance for rotating flow, strong adverse pressure gradient boundary layer flow. Therefore, realizable $k-\varepsilon$ model was selected for the turbulence item. There were both liquid and vapor in the simulation region, which belongs to the two-phase flow. There were three different multiphase flow models in the FLUENT software, such as VOF, Eularian and Mixture. Compared to the other two kind of model, Mixture was commonly used to bubble flow, sedimentation and cyclone separator. Taking into account the bubble flow distribution of ultrasonic cavitation flow field in our simulation, the Mixture model was selected in the multiphase flow, in which the liquid was the main item and the vapor was the second term. There were three kinds of cavitation models in FLUENT software, such as Singhal model, Zwart-Gerber-Belamri model and Schnerr & Sauer model. Schnerr & Sauer model had better stability and robustness and it was not very sensitive to initial conditions. Therefore, the Schnerr & Sauer model was selected for the cavitation model, where the saturated vapor pressure of water was 3540 Pa, and the surface tension coefficient of gas - liquid was 0.0717 N/m . The pressure at the pressure outlet was set to 0 Pa, and the turbulence intensity, turbulence viscosity and time step were set to 0.5, 5 and $1.0 \times 10^{-6} \text{ s}$, respectively. The ultrasonic vibration flow field distribution of specimen surface was divided into two stages, namely the initial stage and the stable stage. After simulation, we found that the stable stage started at $3.999 \times 10^{-3} \text{ s}$. At the same time, the horn is in the middle position and rise with the maximum speed. Then, the horn reaches the top, the middle and the lowest positions at $4.014 \times 10^{-3} \text{ s}$, $4.024 \times 10^{-3} \text{ s}$ and $4.039 \times 10^{-3} \text{ s}$ in turn. Lastly, the horn returned to the middle again at $4.049 \times 10^{-3} \text{ s}$. In this paper, plane, triangle texture and rectangular texture surface were chosen to study by numerical simulation methods. Schematic diagram of the three kinds of surfaces were shown in Fig. 1, in which P, W and H denote texture period, groove width and groove depth, respectively.

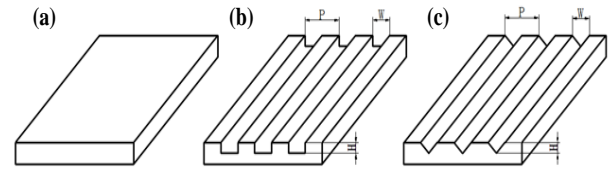


Fig. 1 Schematic diagram of three kinds of surfaces; (a) Plane; (b) Rectangular texture surface; (c) Triangle texture surface.

The specimen with textures was fabricated on the surface of 1060 high purity aluminum plate with the size of $35 \text{ mm} \times 35 \text{ mm} \times 0.6 \text{ mm}$ by laser microfabrication platform, which was shown in Fig. 2a. The ultraviolet nanosecond laser, which has a small thermal influence area and a small influence on the matrix material outside the ablation area, was suitable for the microfabrication of metal materials. In addition, compared with the ultrashort pulse laser, nanosecond laser has lower cost. Therefore, a Nd:YAG solid laser (Model: DSH-355-10) with 355 nm wavelength, 25 ns pulse width, and 6868 Hz pulse frequency was used as the exposure source. The laser power of 520 mW, traversing speed of 5.08 mm/s and focus diameter of 0.015 mm were adopted in fabricating microscale textures. The scanning path of laser focus can be achieved by laser marker controlled by MarkingMate software, which was a laser marking software and had high stability, accuracy and marking efficiency. By changing the scanning path and the number of scanning, the specimen surface with approximate rectangular and triangle microscale textures can be fabricated. Fig. 3b showed the SEM image and partial enlargement of the rectangular texture surface. The 3D profile and section curve of two kinds of microstructure surfaces were shown in Fig. 3c and Fig. 3d respectively. The laser fabricating parameters of the rectangular texture surface: the line spacing of scanning was 0.005 mm and the number of laser scanning was 7. The laser fabricating parameters of the triangle texture surface: the number of laser scanning was 2 for the same line. Thus, it can be seen that the rectangular microgroove and triangle microgroove after laser processing were similar to the regular texture surface.

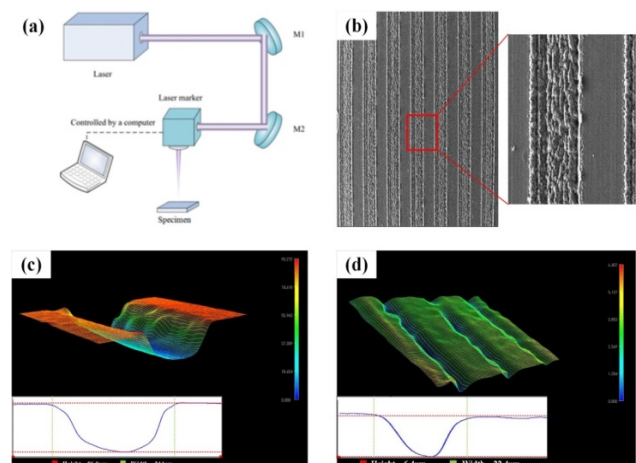


Fig. 2 Laser microfabrication platform and textured surfaces; (a) Schematic diagram of platform; (b) SEM images of rectangular texture surface; (c) 3D profile and section curve of rectangular texture surface; (d) 3D profile and section curve of triangle texture surface.

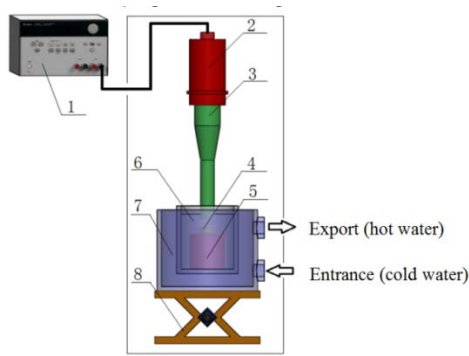


Fig. 3 Schematic diagrams of ultrasonic vibratory cavitation erosion apparatus

For decreasing the influence of particles induced by laser fabrication on cavitation erosion loss, before cavitation erosion experiments, laser textured specimen was ultrasonic cleaned to remove the laser ablated particles. In addition, before and after the cavitation erosion experiments, textured and plane specimens were ultrasonic cleaned in acetone for 5 min, dried in the oven at 105 °C for 10 min and weigh three times to calculate the average value with 0.1 mg analytical balances. Therefore, the mass losses of each erosion experiment can be calculated according to the difference of two average values. The cavitation erosion experiments were carried out on an ultrasonic vibratory apparatus (Model: SLQS 1000), which was shown in Fig. 3. It mainly consists of ultrasonic power supply (1), transducer (2), horn (3), specimen (4), specimen holder (5), reaction vessels (6), thermostats (7) and lift table (8). Deionized water of 25 °C was used as the media in the cavitation erosion experiments. The frequency and peak-to-peak amplitude of transducers were 20 KHz and 0.025 mm respectively. The height of the test liquid was 100 mm and the specimen immersion depth was 12 mm. The horns and the distance between the horns tip and test specimen were 15.9 mm and 2 mm.

3. Results and Discussions

3.1 Cavitation erosion mechanisms

In order to analyze the flow field characteristics of stable stage, the changes of pressure, velocity and gas volume fraction after 3.999×10^{-3} s were shown in Fig. 4. From the pressure distribution shown in Fig. 4a, we found that, compared to the center region, the region of 6 mm radius from the specimen center had lower pressure while the horn moves upwards and this position also shows higher pressure while the horn falls, which leads to serious cavitation erosion in this region. However, curves of the velocity and vapor volume fraction showed only minor changes during a cycle. As shown in Fig. 4b, the curve of velocity distribution had wave peak at the position of about 6 mm radius, in which the largest fluctuation happens during one cycle. However, for the center region of within 4 mm radius, velocity distribution was uniform and its value was not more than 0.1 m/s. Therefore, the bubbles in this region were more stable and belong to the fixed bubble. Fig. 4c indicated that the vapor volume fraction was uniform and about 0.14 in the center region, and had wave peak (about 0.08) in the region of 6 mm radius. In summary, the pressure, velocity and gas volume fraction

distribution on the specimen surface have two distinct regions: the one is the circular region within 4 mm radius and the other is the annular region of 6 mm radius away from the specimen center.

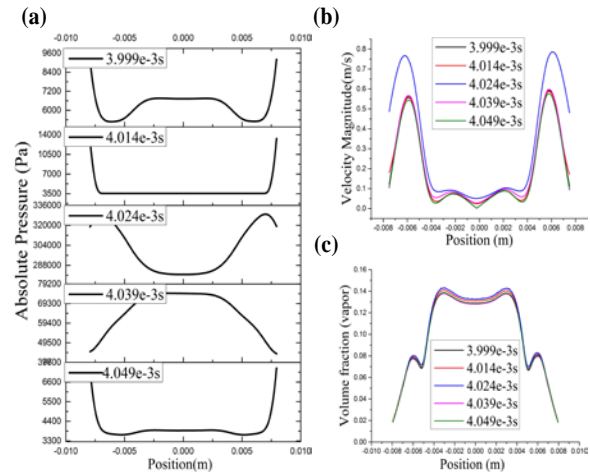


Fig. 4 The flow field distribution in a cycle at the cavitation stabilization phase; (a) Pressure distribution; (b) Velocity distribution; (c) Vapor volume fraction distribution.

Cavitation erosion experiments proved the cavitation damage in the circular and annular areas of the texture surface described by the simulation. Fig. 5 showed SEM images of rectangular texture surface after cavitation erosion for 60 min and numerical simulation results of flow field distribution at the cavitation stabilization phase. In the circular region (Fig. 5a), cavitation pits formed both inside and outside of the grooves. In addition to a relatively larger pit, cavitation erosion was very serious outside of the grooves, and the shape of cavitation pits were regular round. Fig. 5b indicated that the locations of the cavitation erosion were at annular region, and had the trend of expanding outward. The above phenomenon was determined by the flow field distribution beneath the horn. The vapor volume fraction distribution was relatively uniform in the circular region. Fig. 5c shows the numerical simulation results of the velocity, pressure and vapor volume fraction at the time when the horn starts to rise during the cavitation stabilization phase. These red, blue and black lines indicate the pressure distribution on the surface, the velocity distribution at the position of 0.1 mm apart from the specimen surface and the vapor volume fraction distribution respectively. There were higher points for the velocity and vapor volume fraction, and lower point for the pressure in the annular region of 6 mm radius, where the minimum pressure value was 3640 Pa (around the saturated vapor pressure of the water vapor) and the vapor volume fraction was 0.08. Therefore, the accumulation and the fusion of bubbles result in the formation of larger bubbles, produce stronger water jet and shock wave impaction when larger bubbles collapse secondly, and lead to the serious cavitation erosion near the annular region. However, the pressure was relatively uniform (3881 Pa) near the circular region, where the velocity equals zero and fixed type bubbles forms at any time. Therefore, regardless of the rising and falling of horn, there were a part of bubble collapse and dense cavitation

pits in the circular region. Fig. 5d shows the numerical simulation results of flow field distribution inside and outside of the groove, in which black line presented liquid trail. The vortex and cavitation generated on the side of the groove facing the direction of water flow. In addition, because of first decrease and subsequent increase of water when the water flows through the groove and the maximum pressure in the side of the groove, a large number of bubbles were more likely to collapse here and destroy the side of the grooves, as shown in Fig. 5b.

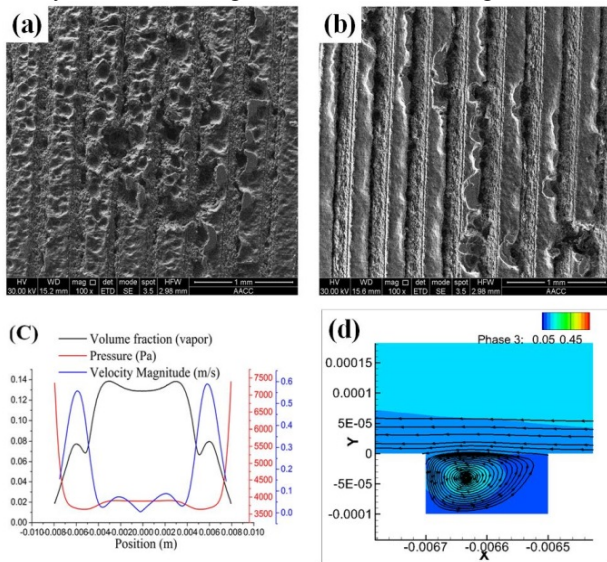


Fig. 5 SEM images of rectangular texture surfaces after cavitation erosion for 60 min and numerical simulation results of flow field distribution at the cavitation stabilization phase; (a) SEM image in the circular region; (b) SEM image in the circular region; (c) Pressure, velocity and vapor volume fraction distribution; (d) Picture of liquid trail in groove in the circular region.

3.2 Effect of microscale texture periods on cavitation erosion

As an important parameter of the microscale texture surface, its period was an important factor that affects the performance of cavitation erosion assistance. In this section, the numerical simulation method using FLUENT software was adopted to investigate the effects of microscale texture periods on the flow field distribution. Fig. 6 showed the numerical simulation results of the influence of rectangular texture surfaces with different periods on flow field at 5.0×10^{-4} s. When the rising horn is at the maximum speed, the cavitation is the most serious. At this time, the pressure distributions of rectangular texture surfaces with the periods of 250 μm , 400 μm , 600 μm were shown in Fig. 6a and Fig. 6b. For the pressure distributions, the overall trends of three different surfaces were similar. The surface of 600 μm period had the lowest pressure, which reached the saturated vapor pressure of water and will cause cavitation, but the minimum pressures for the surfaces with 250 μm and 400 μm periods did not reach that value and cavitation will not happen. In addition, larger region with low pressure for the surface of 600 μm period will cause the accumulation and growth of bubbles. Fig. 6c and Fig. 6d present the vapor volume fraction distributions of three different surfaces. The results indicated that the surface with 600 μm period had the highest peak volume, and which was followed by the

surfaces of 400 μm and 250 μm periods. Therefore, we concluded that the periods of the rectangular texture surface will influence on the overall pressure distribution. The increasing period will induce the decrease of pressure, and lastly cause the generation and growth of the bubbles. On the other hand, with the increase of the period, the fluctuation amplitude of pressure in a single groove decreases, which will inhibit the contraction and collapse of the bubbles.

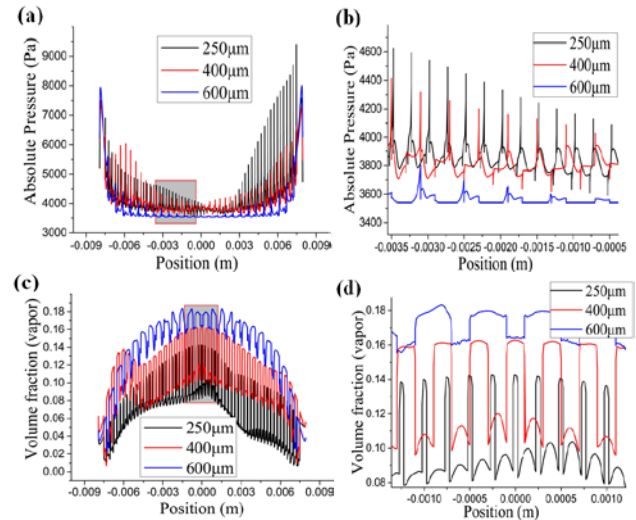


Fig. 6 Numerical simulation results of the influence of rectangular texture with different periods on cavitation; (a) Pressure distribution of different texture periods; (b) Enlarge figure of Fig. 6a; (c) Vapor volume fraction distribution of different texture periods; (d) Enlarge figure of Fig. 6c.

The dual effects of the period on cavitation indicate that it has an optimal value. Therefore, subsequent experiments were carried out to investigate the effects of periods on cavitation erosion and find the optimal period of textured surface. Fig. 7 showed the experimental results of effects of periods on cavitation erosion for the triangle and rectangular texture surfaces. Fig. 7a indicated the results of triangle texture surfaces with periods of 10, 25, 50, 75, 100, 125, 150 and 175 μm . As the periods increase, the cavitation erosion loss decreased first and then increased. There is the minimum value when the period equals to 75 μm . Fig. 7b showed the results of rectangular texture surfaces with periods of 250, 300, 350, 400, 450, 500, 550 and 600 μm . Compared to the results of triangle texture surfaces, rectangular texture surfaces also have similar trend of cavitation erosion loss. Therefore, there are the optimal periods of 75 μm and 400 μm for both triangle and rectangular texture surfaces, respectively.

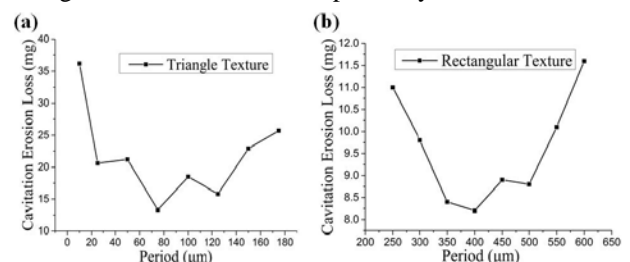


Fig. 7 Experimental results of cavitation erosion loss for both triangle and rectangular texture surfaces; (a) Triangle texture; (b) Rectangular texture.

3.3 Effect of microscale texture types on cavitation erosion

Fig. 8 showed the cavitation erosion experimental results of three kinds of surfaces (Triangle texture surface, rectangular texture surface and plane). The periods of triangle and rectangular texture surfaces are 75 μm and 400 μm . For each type of surface, cavitation erosion experiments were carried out for 30 min, 60 min, 90 min and 120 min, respectively. Fig. 8a showed cavitation erosion loss versus time of three kinds of surfaces. The cavitation erosion losses of the triangle and rectangular texture surfaces slowed down after 30 min, but it started to slow down after 60 min for the plane. During the first 30 min, the cavitation velocity was the largest one for the triangle texture surface and was the smallest one for rectangular texture surface. Therefore, compared to the plane and triangle texture surface, rectangular texture surface had the best performance of cavitation erosion resistance. Figure 8b showed image of rectangular texture surface before cavitation erosion. Fig.8 c-h presented the cavitation erosion morphologies of three kinds of surfaces after 60 min and 120 min. We found that the cavitation erosion with larger pits occurred in the annular region rather than the circular region, and that with many dense and small pits in the circular region. However, rectangular microstructure surface had the least pits after cavitation erosion experiments of 120 min, which manifested that rectangular textures had the best performance of cavitation erosion resistance.

The above experimental results were similar to the following numerical simulation results (Fig. 9), which presented the flow field of three kinds of surfaces at 5.0×10^{-4} s. As the pressure distribution shown in Fig. 9a and Fig. 9b, we found that the pressures on both the rectangular and triangle texture surfaces had some fluctuation, which were the same to the overall tendency of plane. While ignoring the instantaneous vibration, pressure fluctuation on rectangular texture surface was similar to the Cosine curve and its peak value also below the pressure of plane. Pressure curve of triangle texture surface also had large peak value. However, its interval of high pressure and low pressure cover a longer distance compared to that of rectangular texture surface, which provide a growth and collapse time ranges for swimming type bubbles. In addition, pressure fluctuation for both the rectangular and triangle texture surfaces was larger in the annular region, which was easy to make the bubbles instability and collapse. Fig. 9c and Fig. 9d demonstrated the vapor volume fraction distributions of three kinds of surfaces. We found that both texture surfaces will result in the fluctuation of gas volume fraction on specimen surfaces and the gas volume fraction of rectangular texture surface was smaller than that of plane and triangle texture surface wholly. Although the rectangular texture surface can cause the fluctuation of the vapor volume fraction at different positions of the specimen, its cavitation degree was lower. Therefore, compared to the plane, rectangular texture surfaces had better cavitation erosion resistance. Based on the above experimental and numerical simulation results, we concluded that rectangular texture surface had better performance of cavitation erosion resistance compared to the other two surfaces.

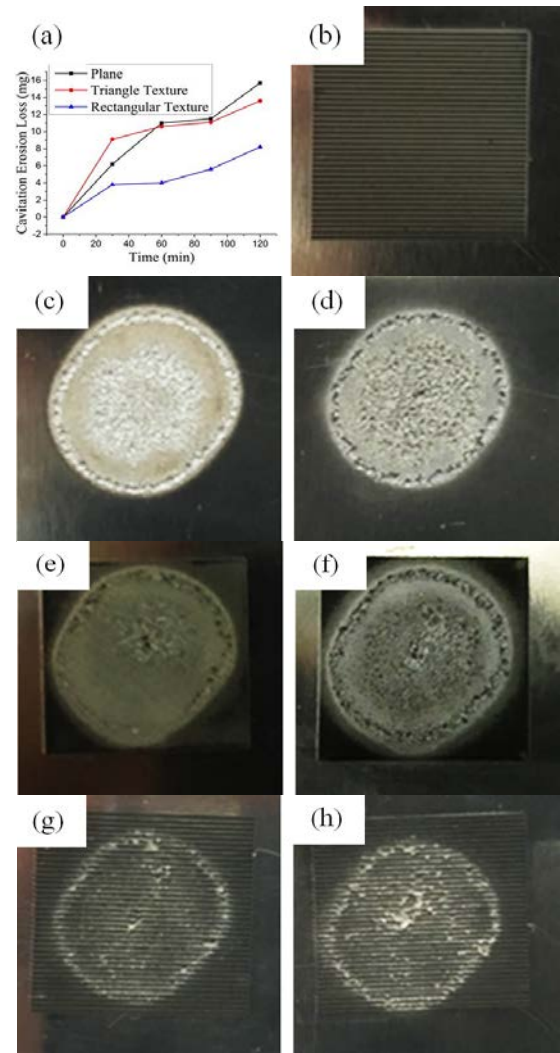


Fig. 8 Cavitation erosion experimental results of three kinds of surfaces; (a) Cavitation erosion loss versus time; (b) Picture of rectangular texture before cavitation erosion (c) and (d) Cavitation erosion morphology of plane after 60 min and 120 min; (e) and (f) Cavitation erosion morphology of triangle texture surface after 60 min and 120 min; (g) and (h) Cavitation erosion morphology of rectangular texture surface after 60 min and 120 min.

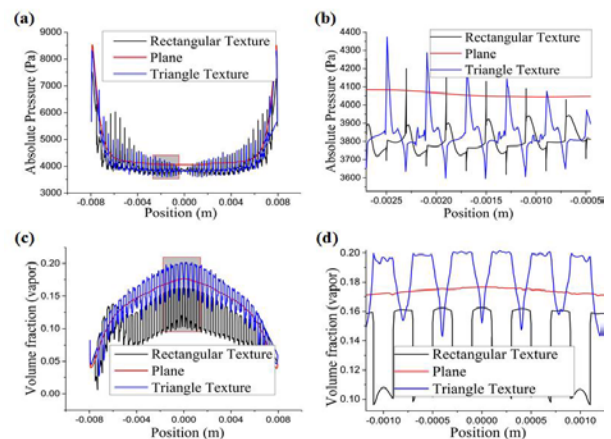


Fig. 9 Cavitation numerical simulation results of three kinds of surfaces; (a) Pressure distribution; (b) Enlarge figure of Fig. 9a; (c) Vapor volume fraction distribution; (d) Enlarge figure of Fig. 9c.

The effect of surface chemistry formation of hard surface oxides could be relevant to the cavitation erosion of laser induced microscale texture surfaces. It is proved that the surface of hard material has better anti-cavitation performance [15, 16]. Fig. 10 showed the cavitation erosion of four kinds of surfaces after 60 min cavitation erosion experiments. The surface roughness of plane was approximately 0.14 μm , whereas the roughness of laser induced rough surface was 0.35 μm . Compared with the plane, triangle and rectangular surfaces, the cavitation erosion loss of laser induced rough surface was the largest one, reaching 18.3 mg. In spite of the oxidizing and hardening, laser induced rough surface, compared to the plane, was easy to be destroyed because of its random rough structure. There results were consistent with that of Lu's researches [17]. Therefore, the cavitation erosion of the texture surface in this paper is mainly attributed to the change of flow field characteristics.

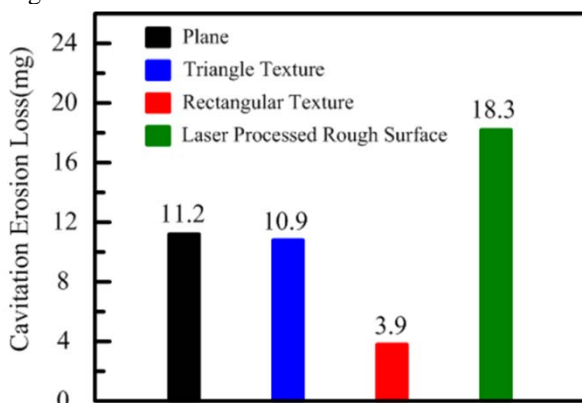


Fig. 10 Cavitation erosion loss after 60min of four kinds of surfaces

4. Conclusion

In this paper, cavitation erosion behavior of plane and both laser induced microscale texture surfaces were investigated by experimental and numerical simulation methods. The conclusions as follows:

(1) In the cavitation stabilization phase, the pressure, velocity and gas volume fraction distributions on the specimen surfaces have two distinct regions: the one is the circular region within 4 mm radius and the other is the annular region of 6 mm radius away from the specimen center. In the annular region the accumulation and the fusion of bubbles result in the formation of larger bubbles, produce stronger water jet and shock wave impaction, and leads to the serious cavitation erosion in the end. However, in the circular region, the velocity equals zero and bubbles with fixed type forms at any time. There only had a part of bubbles collapse and dense cavitation erosion pits.

(2) The increasing period of the rectangular texture surface will induce the decrease of pressure, and cause the generation and growth of the bubbles. On the other hand, with the increase of the period, the fluctuation amplitude of pressure in a single groove decreases, which will inhibit the contraction and collapse of the bubbles. Thus, the dual effects of the period on cavitation indicate that there has an optimal value. Experimental results proved that optimal periods for both triangle and rectangular texture surfaces were 75 μm and 400 μm , respectively.

(3) Both microscale texture surfaces result in the fluctuation of gas volume fraction on specimen surface and the gas volume fraction of rectangular texture surface was smaller than that of plane and the triangle texture surface. Although the rectangular texture surface can cause the fluctuation of the vapor volume fraction at different positions of the specimen, its cavitation degree was lower. Therefore, rectangular texture surface had better cavitation erosion resistance.

Acknowledgements

The author gratefully acknowledges Research project of Xuzhou University of Technology (XKY2017228), the Discipline Research Initiative of CUMT (2015XKQY12) and A Project Funded by the Priority Academic Program Development of Jiangsu Higher Education Institutions (PAPD) for supporting this work.

References

- [1] Grewal H. S, Pendyala. Prashant, and Shin. Hyogeun: *Wear*, 384, (2017) 151.
- [2] Luo. Y, Zhang. D, and Xu. X: *Surf. Eng*, 32, (2016) 119.
- [3] Cai. Chujiang, Sang. Nannan, and Teng. Sicong: *Surf. Coat. Tech.*, 307, (2016) 366.
- [4] Kawasegi. Noritaka, Ozaki. Kazuma, and Morita. Noboru: *Precision Engineering*, 47, (2017) 311.
- [5] Zhang. Chen, Shi. Guilin, and Ehmann. Kornel F: *Int. J. Mach. Tool. Manu.*, 120, (2017) 72.
- [6] X L. Zhang, X. Wang, and W. Kong: *Appl. Surf. Sci.*, 258, (2011) 113.
- [7] J X Man, H F Yang, and Y Q Wang: *J. Laser. Micro. Nanoen.*, 12, (2017) 16.
- [8] Yang H F, He H D, and Zhao E L: *Laser.Phys. Lett.*, 11, (2014) 105901.
- [9] H F Yang, T C Chen, and J G Qian: *B .Mater. Sci*, 38, (2015) 173.
- [10] L. Zhang, Y K. Zhang, and J Z. Lu: *Corros. Sci*, 66, (2013) 5.
- [11] Alicja K. Krella: *Surf. Coat. Tech*, 228, (2013) 115.
- [12] X Gong, W He, and Z Li: *Ceram.Int.*, 40, (2014) 7161.
- [13] Li. H B, Cui Z D, and Li Z Y: *Appl. Surf. Sci.*, 298, (2014) 164.
- [14] Chen H S, Li Y J, and Chen D R: *Tribol. Lett.*, 26, (2007) 153.
- [15] T. Koppitz, P. Jung, and G. Muller: *J. Nucl. Mater*, 343, (2005) 92.
- [16] K.H. Lo, F.T. Cheng, and H.C. Man: *Surf.Coat. Tech*, 173, (2003) 96.
- [17] J. Lu, K.-H.ZumGahr, and J.Schneider: *Wear*, 265, (2008) 1680.

(Received: June 9, 2018, Accepted: October 25, 2018)